Tilted and crossing vortex chains in layered superconductors

A. E. Koshelev

Materials Science Division, Argonne National Laboratory,Argonne, Illinois 60439

In the presence of the Josephson vortex lattice in layered superconductors, a small c-axis magnetic field penetrates in the form of vortex chains. In general, the structure of a single chain is determined by the ratio of the London [λ] and Josephson [λ_J] lengths, $\alpha = \lambda/\lambda_J$. The chain is composed of tilted vortices at large α's (tilted chain) and at small α's it consists of a crossing array of Josephson vortices and pancake-vortex stacks (crossing chain). We study chain structures at intermediate α's and found two types of phase transitions. For $\alpha \lesssim 0.6$ the ground state is given by the crossing chain in a wide range of pancake separations $a \gtrsim [2-3]\lambda_J$. However, due to attractive coupling between deformed pancake stacks, the equilibrium separation can not exceed some maximum value depending on the in-plane field and α. The first phase transition takes place with decreasing pancake-stack separation a at $a = [1-2]\lambda_J$, and rather wide range of the ratio α, $0.4 \lesssim \alpha \lesssim 0.65$. With decreasing a, the crossing chain goes through intermediate strongly-deformed configurations and smoothly transforms into a tilted chain via a second-order phase transition. Another phase transition occurs at very small densities of pancake vortices, $a \sim [20-30]\lambda_J$, and only when α exceeds a certain critical value ~ 0.5. In this case a small c-axis field penetrates in the form of kinks. However, at very small concentration of kinks, the kinked chains are replaced with strongly deformed crossing chains via a first-order phase transition. This transition is accompanied by a very large jump in the pancake density.

PACS numbers: 74.25.Qt, 74.25.Op, 74.20.De

1. INTRODUCTION

Layered superconductors have an amazingly rich phase diagram in tilted magnetic field. Point (or "pancake") vortices generated by the c-axis com-

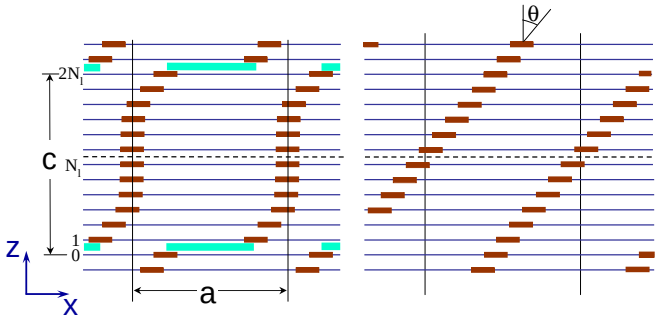

Fig. 1. Crossing (left) and tilted (right) vortex chains.

ponent of the magnetic field [1] can form a vast variety of lattice structures. Possible structures include the kinked lattice, [2,3,4,5], tilted vortex chains [6], coexisting lattices with different orientation[7] and crossing lattices composed of sublattices of Josephson vortices (JVs) and pancake-vortex stacks[3,8]. The main source of such richness is the existence of two very different kinds of interactions between the pancake vortices in different layers: magnetic and Josephson interactions. The key parameter, which determines the relative strength of these two interactions and plays a major role in selecting the lattice structures, is the ratio of the two fundamental lengths, the in-plane London penetration depth, $\lambda \equiv \lambda_{ab}$, and Josephson length $\lambda_J = \gamma s$, with γ being the anisotropy parameter and s being the interlayer spacing, $\alpha = \lambda/\lambda_J$. One can distinguish two limiting cases which we refer to as "extremely anisotropic" case, $\alpha < 0.4$, and "moderately anisotropic" case $\alpha > 0.7$. Among known atomically layered superconductors, only $Bi_2Sr_2CaCu_2O_x$ (BSCCO) and related compounds may belong to the "extremely anisotropic" family. Even in this compound the parameter α is not smaller than ~ 0.25 and increases with temperature so that BSCCO typically becomes "moderately anisotropic" in the vicinity of the transition temperature.

At very small c-axis fields (up to 1-2 G) the pancake stacks in layered superconductors within a wide range of anisotropies are arranged in chains. An isolated chain is a two-dimensional array of pancake vortices oriented perpendicular to the layers, see Fig. 1. At somewhat higher fields the chains are surrounded by the regions of regular vortex lattice[9]. The internal structure of an isolated chain depends on the ratio α and it is relatively simple in two limiting cases. At large α the chain is composed of tilted pancake stacks (tilted chain, right picture in Fig. 1) and at small α it consists of crossing arrays of JVs and pancake stacks (crossing chains, left picture in Fig. 1). In this paper we address the highly nontrivial problem of how one

structure transforms into another in the region of intermediate α. We analytically and numerically computed ground state configurations in the isolated vortex chain and found two types of phase transitions. The first phase transition typically takes place for the intermediate separations between pancake stacks a, $a = [1-2]\lambda_J$, and rather wide range of the ratio α, $0.4 \lesssim \alpha \lesssim 0.65$. The ground state is given by the crossing chain in a wide range of pancake separations a. Due to attraction between deformed pancake stacks [10], the equilibrium separation can not exceed some maximum value, which depends on the in-plane field and α and it is typically of the order of several λ_J. With decrease of the pancake separation a, the crossing chain becomes strongly deformed and smoothly transforms into the modulated tilted vortices. The modulation vanishes at a second-order phase transition at which the system transforms into the tilted-chain state. This phase transition provides possible interpretation of the recent Lorentz-microscopy experiment [11] at which it was observed that the pancake stacks located in the chains smear along the chain direction while the pancake stacks outside chains remain well defined. This smearing may indicate transition into the tilted-chain state.

Another phase transition occurs at very small densities of pancake vortices, $a \sim 20 - 30\lambda_J$, and only when α exceeds a certain critical value ≈ 0.5 (exact criterion depends on the in-plane magnetic field). In this case a small c-axis field penetrates in the form of kinks. The kinked vortex lines forming tilted chains are composed of JV pieces separated by kinks[2,3,4]. If the kink energy is only slightly smaller then the energy per pancake in a straight pancake stack then at very small concentration of kinks, typically at $a \approx [20-30]\lambda_J$, the kinked chains are replaced with strongly deformed crossing chains via a first-order phase transition. Due to the opposite signs of interactions (kinks repel and deformed pancake stacks attract each other) this transition is accompanied by a very large jump in the pancake density. With further decrease of the pancake separation the chain smoothly transforms back to the tilted chain as it was described in the previous paragraph.

We constructed the chain phase diagrams for different ratios α. As follows from the above description, there are two types of phase diagrams in the region of intermediate α's:

- In the range $0.4 \lesssim \alpha \lesssim 0.5$ a small c-axis field first penetrates in the form of pancake-stack chains located on JVs. Due to attractive coupling between the deformed stacks, their density jumps from zero to a finite value. With further increase of the c axis field the chain goes through intermediate strongly deformed configurations and smoothly transforms into a tilted chain;

- In the range $0.5 \lesssim \alpha \lesssim 0.65$ small c-axis field first penetrates in the

form of kinks creating kinked tilted vortices. With increase of a c axis field this structure is replaced via the first-order phase transition with the strongly-deformed crossing chains. This transition is accompanied by a large jump of pancake density. Further evolution of the chain structure is identical to the smaller-α scenario: the structure smoothly transforms back into the tilted-chain state.

The exact transition between the two types of behavior depends also on in-plane field. Larger in-plane field favors the first scenario.

The second scenario provides a natural interpretation to recent scanning-Hall-probe observations[12]. It was observed that at very small concentration of pancakes the chains are magnetically homogeneous and separate pancake stacks are not resolved. When the external field exceeds some critical value of the order of several Oersted, crystallites of the pancake stacks are suddenly formed along the chain and the flux density in the crystallites is much higher then the flux density in the homogeneous chains. Our calculations provide consistent interpretation for these observations. The magnetically homogeneous chains are interpreted as kinked/tilted chains (such interpretation has been proposed by Dodgson[13]) and formation of crystallites can be attributed to the low-density [kinked lines]-[crossing chains] first-order phase transition with density jump.

The paper is organized as follows. In Section 2. we consider the chain energy functional. In Section 3. we present analytical estimates for the chain energy in the two limiting cases, crossing and tilted chain, and discuss location of transitional region between these states. In section 4. we review attractive interaction between deformed pancake stacks located on JVs. Section 5. contains the results on numerical exploration of the the phase diagram. We discuss two different phase transitions between the tilted and crossing chains and two types of phase diagrams which are realized in the region of intermediate parameter α.

2. CHAIN ENERGY FUNCTIONAL

In this paper we focus on the structure of an isolated vortex chain with period a in x direction and period $c = Ns$ in z direction where $N = 2N_l$ is the number of layers per vertical chain period (see Figure 1). This corresponds to the tilting angle θ of the magnetic induction with respect to the c axis with $\nu \equiv \tan\theta = a/c$. The pancake separation a is determined by the c-axis field B_z. Note that we consider the region of very small B_z (0.1-5 G), where it is typically much smaller than external field. The vertical period c is fixed by the in-plane field B_x, $c \approx \sqrt{2\Phi_0/(\sqrt{3}\gamma B_x)}$. For BSCCO ($\gamma \sim 500$) this

period is approximately equal to 20 layers at $B_x \approx 50$G. The chains are separated by distance c_y, $c_y = \Phi_0/cB_x \gg c$.

Our calculations are based on the Lawrence-Doniach free-energy functional in the London approximation, $F_{\rm LD}$, (see, e.g., Ref. 3). The chain structure is mainly determined by pancake displacements from aligned positions u_n and regular phase distribution $\phi_{r,n}(x,y)$. We consider the case $c \ll \lambda$ and in-plane distances much smaller than λ_c. In this situation the general Lawrence-Doniach energy, F_{LD}, can be significantly simplified using several approximations: (i)we neglect screening of regular phase and z-axis vector-potential; (ii)we subtract the energy of straight pancake stacks, $(B_x/\Phi_0)\varepsilon_{\rm PS}$, allowing us to eliminate logarithmically diverging pancake-core contributions; (iii)we drop the trivial magnetic energy term $B_x^2/8\pi$ which plays no role in selection between different chain phases. We will use the chain energy per unit area lattice, $E \equiv c_y[F_{\rm LD}/V - B_x^2/(8\pi) - (B_z/\Phi_0)\varepsilon_{\rm PS}]$ with V being the total system volume. With the above assumptions the chain energy functional can be represented as

$$
\begin{aligned}
E = \frac{1}{c}\sum_{n=1}^{N}\int_0^a \frac{dx}{a}\int_{-c_y/2}^{c_y/2} dy \Bigg[& \frac{J}{2}\left(\nabla\phi_{r,n}\right)^2 \\
& + E_J\left(1-\cos\left(\nabla_n\left(\phi_{r,n}+\phi_{v,n}\right) - \frac{2\pi s}{\Phi_0}B_x y\right)\right)\Bigg] \\
& + \frac{1}{2}\frac{N}{N_{tot}}\sum_{n\neq m} U_{Mr}(u_n - u_m, n-m)
\end{aligned}
\tag{1}
$$

where the phase stiffness, J, and the Josephson coupling energy, E_J, are given by

$$
J \equiv \frac{s\varepsilon_0}{\pi},\ E_J \equiv \frac{\varepsilon_0}{\pi s\gamma^2},\ \text{with } \varepsilon_0 \equiv \frac{\Phi_0^2}{(4\pi\lambda)^2}, \tag{2}
$$

$\lambda \equiv \lambda_{ab}$ and λ_c are the components of the London penetration depth and $\gamma = \lambda_c/\lambda_{ab}$. The ratio of the two energy scales determines the most important length scale of the problem, the Josephson length, $\lambda_J = \gamma s = \sqrt{J/E_J}$. $\phi_{v,n}(\mathbf{r})$ is the vortex phase variation induced by displacement of pancake rows, u_n, from the ideally aligned positions

$$
\varphi_{v,n}(x,y;u_n) = \arctan\frac{\tan\left(\pi(x+u_n)/a\right)}{\tanh\left(\pi y/a\right)} - \arctan\frac{\tan\left(\pi x/a\right)}{\tanh\left(\pi y/a\right)}; \tag{3}
$$

the discrete gradient $\nabla_n\phi_n$ is defined as $\nabla_n\phi_n \equiv \phi_{n+1} - \phi_n$. $U_{Mr}(u_n - u_m, n-m)$ is the interaction energy between the pancake rows per unit

length, computed with respect to straight stacks

$$U_{Mr}(u,n) \equiv \frac{1}{a}\sum_m \left[U_M(ma+u,n) - U_M(ma,n)\right],$$

where $U_M(\mathbf{R},n)$ is the magnetic interaction between pancakes[1]

$$U_M(\mathbf{R},n) \approx 2\pi J\left[\ln\frac{L}{R}\left[\delta_n - \frac{s}{2\lambda}\exp\left(-\frac{s|n|}{\lambda}\right)\right] + \frac{s}{4\lambda}u\left(\frac{r}{\lambda},\frac{s|n|}{\lambda}\right)\right] \quad (4)$$
$$u\,(r,z) \equiv \exp(-z)E_1\,(r-z) + \exp(z)E_1\,(r+z)\,,$$

$E_1(u) = \int_u^\infty (\exp(-v)/v)\,dv$ is the integral exponent, $r \equiv \sqrt{R^2+(ns)^2}$, and L is a cutoff length; N_{tot} is the total number of layers.

The energy (1) contains contribution coming from a long-range suppression of the Josephson energy accumulated from distances $c \ll y \ll c_y$, that is identical in all chain phases, $E_{\text{J-LR}} = E_J\pi^2 c_y/(6N^2 s)$. It is convenient to separate this term and define the local chain energy, E^{loc},

$$E^{loc} \equiv E - E_{\text{J-LR}}. \quad (5)$$

This part of energy weakly depends on c_y and does not diverge for $c_y \to \infty$.

We numerically minimized the energy functional (1) with respect to u_n and $\phi_{r,n}(x,y)$ within unit cell, $0 < x < a$, $0 < y < c_y/2$, and $0 < n < N_l = N/2$ using appropriate symmetry and periodic boundary conditions. In calculation of magnetic coupling energy one has to take into account periodic conditions for pancake displacements, $u_{n+N} = u_n$. In addition, if one selects z axis origin at the center of the JV then symmetry also requires $u_{-n} = -u_n$. Two simple limiting cases in Fig. 1 correspond to (i) $u_n \ll a$ for the crossing chain and (ii) $u_n = -a(1-(n-1/2)/N_l)/2$ for the tilted chain.

3. CHAIN ENERGIES IN LIMITING CASES

Analytic estimates for energy contributions are possible in two limiting cases of weakly deformed crossing chain and tilted chain shown at Fig. 1. In this section we summarize results for chain energies in different limits. Detailed derivations will be published elsewhere.

Local energy of crossing chain per unit area is given by

$$E_{CL}^{loc} = \frac{\varepsilon_0}{a}\left(\frac{\nu}{\gamma}\left(\ln N - 0.41\right) - \frac{8\alpha^2}{\ln(3.5/\alpha)N}\right), \quad (6)$$

Here the first term represents the local JV energy, E_{JV}^{loc}, and the second term is the contribution from the crossing energies of JVs and pancake stacks[8].

The local tilted-chain energy per unit area in the limit $\nu \equiv \tan\theta \ll \gamma$ is given by

$$E_{TV}^{loc} = \frac{\varepsilon_0}{a}\left[U\left(\frac{a}{2\pi\lambda}\right) + \frac{\nu^2}{2\gamma^2}\left(\ln N - 0.95\right)\right], \tag{7}$$

$$\text{where } U(x) = \sum_{m=1}^{\infty}\left(\frac{1}{m} - \frac{1}{\sqrt{m^2+x^2}}\right) = \begin{cases} \zeta(3)x^2/2, \ x \lesssim 0.5 \\ \frac{1}{2x} - \ln\frac{2}{x} + \gamma_E, \ x \gtrsim 1 \end{cases},$$

with $\gamma_E \approx 0.5772$ being the Euler constant. In Eq. (7) the first term represents the loss of the magnetic coupling energy in the tilted chain and the second term represents the Josephson energy loss.

In the region of kinked lines $\nu \gg \gamma$ (but $\nu \ll N\gamma/2\pi$), the local chain energy is given by

$$E_{TV}^{loc} \approx E_{JV}^{loc} + \frac{\varepsilon_0}{a}\left[\ln\frac{0.44}{\alpha} + \frac{\gamma}{2\nu}\left(\ln\left(\frac{\gamma N}{\nu}\right) - 2.454\right)\right]. \tag{8}$$

In this equation E_{JV}^{loc} is the local JV-lattice energy, the first term in square brackets gives the single-kink energy and the third term gives the kink interaction energy.

To find out whether the crossing or tilted chain is realized for given values of parameters a, c, and α, we have to compare the energies of these states. Comparison of Eqs. (6) and (7) gives transitional pancake separation a_c which decreases with N and increases with α [14]. Naively, one may think that intersection of the energy curves for two states would correspond to a first-order phase transition between these states. However, as we will see from numerical simulations, in the region $\nu = \tan\theta < \gamma$ another scenario is realized. Typically, strongly deformed intermediate chain configurations develop in the transitional region providing a smooth transformation between the two limiting configurations. Therefore, a simple energy comparison gives only an approximate location of the transitional region separating the two configurations.

In the region $1 < \nu/\gamma < N/2\pi$ and $a > 2\pi\lambda$ comparison of the energies (6) and (8) gives the following equation

$$\ln\frac{1}{\alpha} - 0.81 + \frac{\gamma}{2\nu}\left(\ln\left(\frac{\gamma N}{\nu}\right) - 2.454\right) + \frac{8\alpha^2}{\ln(3.5/\alpha)N} = 0 \tag{9}$$

This equation has a solution only in the kink penetration regime, $\ln(1/\alpha) - 0.81 < 0$, where the kink energy is only slightly smaller that the energy per pancake of a straight pancake-vortex stack. In contrast to the case $\nu \ll \gamma$, this equation does correspond to a very strong first-order phase transition.

4. ATTRACTION BETWEEN DEFORMED PANCAKE STACKS. MAXIMUM EQUILIBRIUM SEPARATION

A peculiar property of the crossing chain is an attractive interaction between the deformed pancake stacks at large distances[10]. As a consequence, when the magnetic field is tilted from the direction of layers the density of pancake stacks located on JVs jumps from zero to a finite value. This means the existence of a maximum equilibrium separation a_m between pancake stacks, i.e., chains with $a > a_m$ are not realized in equilibrium. Note that the tilted vortices also attract each other within some range of angles and distances [6] meaning that tilted chains also have this property in some range of parameters.

Simple analytical formula for the attraction energy between the deformed pancake stacks can be derived for very anisotropic superconductors $\lambda_J \gg \lambda$ in the range $\lambda \ll R \ll \lambda_J$ [10]. In this limit short-range pancake displacements u_n from the aligned positions in two neighboring stacks produce dipole-like contribution to interaction energy per unit length between these stacks $\delta U_i(R) = -2\varepsilon_0 \left\langle u^2 \right\rangle / R^2$. This term has to be combined with the usual repulsive interaction between straight stacks $U_{i0}(R) = 2\varepsilon_0 \mathrm{K}_0(R/\lambda) \approx 2\varepsilon_0 \sqrt{\pi\lambda/2R} \exp(-R/\lambda)$. Minimum of the total interaction energy, $U_{i0}(R) + \delta U_i(R)$ gives an estimate for the maximum equilibrium separation a_m [10], $a_m = \lambda \ln(C\lambda^2/\left\langle u^2 \right\rangle)$ and this result is valid until $a_m < \lambda_J$. Because in BSCCO λ_J is only $2-3$ times larger than λ, this simple formula is not practical for this compound. We will see that a_m in BSCCO is usually larger than λ_J. In general, the maximum equilibrium separation a_m is determined by the minimum of the pancake part of energy per one stack $U(a) = a\,(E(a) - E(\infty))$. When the main contribution to the total interaction energy is coming from the nearest-neighbor interaction, a_m coincides with the position of the minimum in the pair interaction potential.

5. NUMERICAL EXPLORATION OF CHAIN STRUCTURES

We explored the chain structures by numerically minimizing (1) with respect to the pancake row displacement u_n and regular phase distribution $\phi_{r,n}$ for different values of the parameters a, $N = 2N_l$, and α. In the following sections we review the results of these calculations.

5.1. Phase Transition From Crossing To Tilted Chains With Decreasing Pancake Separation

We studied the evolution of chain structures with decreasing pancake separation a at fixed α and N. For small values of α we found that the chain structure smoothly evolves with decreasing a from crossing to tilted configuration. An example of such evolution is presented in Fig. 2 for $N = 14$ and $\alpha = 0.4$. The upper plot shows the dependence of the maximum pancake displacement from the straight-stack position u_{max}/a (defined in the inset) on the pancake separation a. We will use this parameter to characterize the chain structure throughout the paper. It changes from zero for straight stacks to $(1-1/N)/2$ for tilted chains. The lower plot shows the a dependence of the reduced pancake energy per unit cell, $U \equiv ca(E(a) - E(\infty))/J$, which is used to determine the maximum equilibrium separation a_m. At large a a weakly deformed crossing configuration is realized (see structure at $a = 3\lambda_J$). With decrease of a the chain evolves into strongly corrugated configurations such as configuration for $a = 2\lambda_J$ in Fig. 2. With further decrease of a this structure smoothly transforms into modulated tilted lines (see structure for $a = 1.5\lambda_J$). Finally, the last structure transforms via a second-order phase transition into the straight tilted lines. For parameters used in Fig. 2 this occurs at $a = 1.3\lambda_J$. The plateau in the dependence $u_{max}(a)/a$ below this value of a corresponds the maximum possible relative displacement $(1 - 1/N)/2 \approx 0.4643$ in the tilted chain.

Comparison of numerical and analytical calculations shows that the analytical estimates (6) and (7) accurately reproduce numerical results for the weakly deformed crossing chain and for the tilted chain. However, the numerical study predicts intermediate configurations with energies smaller than the energies of the both limiting configurations. As a result, a naively expected first-order phase transition is replaced by a continuous transition occurring at significantly smaller a. The transitional region just marks the location of the intermediate strongly deformed chain configurations. The observed continuous phase transition is related to the instability of isolated tilted vortices in anisotropic superconductors[16,15].

In Fig. 3 we present the chain phase diagrams in the a-N-plane for $\alpha = 0.4$. The thick line shows the phase transition into the tilted-chain state. One can see that at larger N the transition takes place at smaller a. With increase of α this line moves higher. Dotted lines show locations of the maximum equilibrium separation a_m discussed in Sec. 4.. We see that $a_m(N)$ line crosses the transition line meaning that at small N a_m falls into the tilted-chain region and at large N it falls into the crossing-chain region. The obtained phase diagram implies that at small tilting angle of

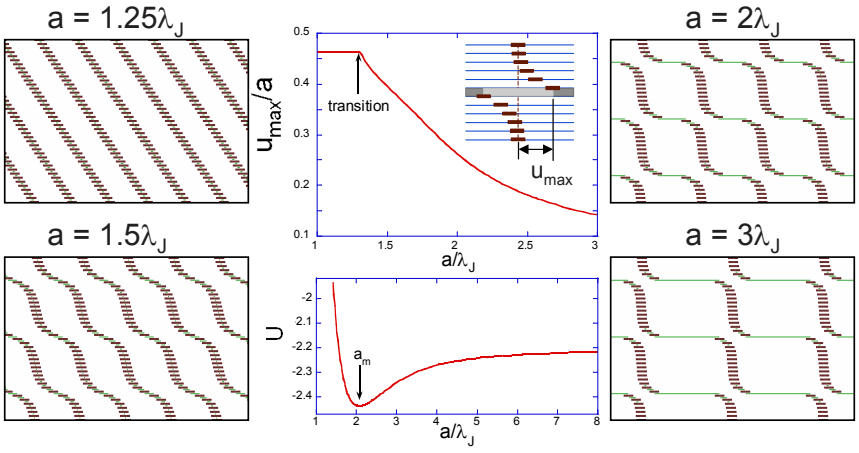

Fig. 2. *Upper plot* shows the dependence of the maximum displacement(defined in the inset) on pancake separation a for $N = 14$ and $\alpha = 0.4$. *Lower plot* shows dependence of the pancake energy per unit cell U (in units of phase stiffness J) on pancake separation. Its minimum determines the maximum equilibrium separation a_m. Representative chain structures are shown for several values of a(boxes show positions of the pancake vortices and horizontal lines mark JVs). One can see that the system evolves from weakly deformed chain ($a = 3\lambda_J$) via strongly deformed chain ($\alpha = 2\lambda_J$) to modulated tilted chain ($\alpha = 1.5\lambda_J$). The last structure transforms via a 2nd-order phase transition at $\alpha = 1.3\lambda_J$ into tilted straight vortices.

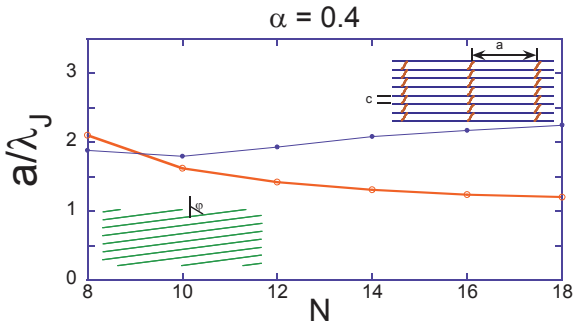

Fig. 3. Chain phase diagrams in the plane $a/\lambda_J - N$ for the ratio $\alpha = 0.4$. Thick line with open circles indicates phase transition into the tilted chain. Thin line shows the maximum equilibrium separation a_m.

the field (corresponding to small a) the tilted chains have lower energy than the crossing chains. This is similar to the situation at higher fields, in the dense lattice, where the crossing-lattices state also is expected to transform into the simple tilted lattice at small tilting angle of the field[8].

5.2. Reentrant Transition To Kinked/Tilted Lines At Small Concentration Of Pancakes At $\alpha \gtrsim 0.5$

At higher values of the ratio α a new qualitative feature appears in the phase diagram. When α exceeds the critical value, the c axis field initially penetrates in the form of kinks forming kinked vortex lines (lock-in transition[2,4,3]). The critical value of α is determined by combination of numerical constants in the pancake-stack and kink energies. At present, our best estimate for this constant is $\alpha_c \approx 0.44$. The critical value of α increases with decrease of N, due to the increasing relative contribution of the crossing energies in the energy of crossing chain. A very peculiar behavior is expected when α only slightly exceeds α_c. The competing chain states have very different interactions: deformed stacks attract and kinks repel each other. Moreover, at the same value of the c-axis magnetic induction, B_z, the kinks are much closer than the stacks and the absolute value of the kink interaction energy is much larger than the interaction energy between deformed stacks. As a consequence, with increase of B_z the total energy of the kinked lines rapidly exceeds the total energy of the crossing chain and the system experiences a first-order phase transition into the crossing-chain state. Due to the attractive interaction between the pancake stacks, the pancake/kink separation at which the energy curves cross does not give the equilibrium separation for the crossing chain and the stack separation jumps at the transition to a value slightly smaller than the maximum equilibrium separation a_m. This means that the phase transition is accompanied by jumps of the pancake density and magnetic induction, B_z.

This behavior was confirmed by numerical calculations. Figure 4 shows a plot of the dependence of the energy per chain unit cell $\mathcal{U}$ on the pancake density $n = 1/a$ for $N = 16$ and $\alpha = 0.6$. This dependence has two branches, corresponding to two different starting states at small n, crossing chain and kinked lines, and the kinked vortex lines have smaller energy at smaller n. The branches cross at $n = 0.068$ marking the first-order transition. The variations of $\mathcal{U}$ at small n occur due to the interaction energy and one can see that the kink interaction energy is much larger than the crossing-chain interaction energy. With further increase of n, the crossing chain smoothly transforms into the tilted chain following the scenario described in the pre-

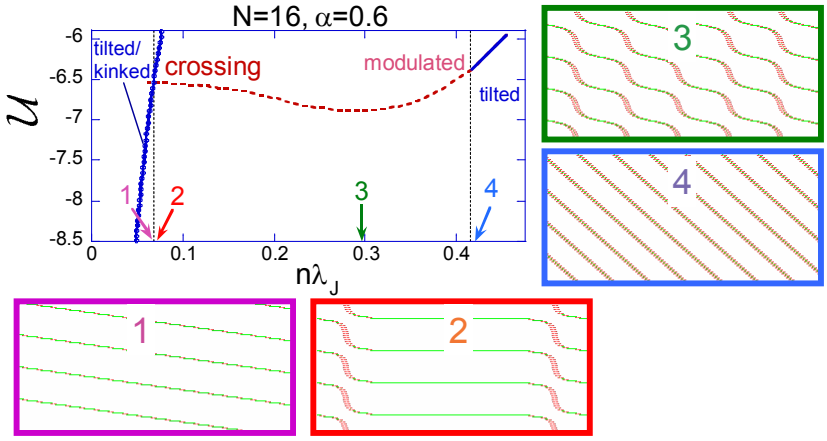

Fig. 4. The dependence of the pancake energy per chain unit cell on pancake density $n = 1/a$ for $N = 16$ and $\alpha = 0.6$. The two branches at low n correspond to two different starting states, kinked lines (1) and crossing chain (2). The kinked lines have lower energy at very small n, at $n < 0.068$. Crossing chain smoothly transforms back into tilted chain with increase of n. The transformation is completed at the second-order phase transition point near $n\lambda_J = 0.4$. Chain configurations are shown at four marked points.

vious Section. The second-order phase transition for these parameters takes place at $n \approx 0.4$ corresponding to $a \approx 2.5\lambda_J$. The latter value is somewhat smaller than the maximum equilibrium separation $a_m \approx 3.44\lambda_J$.

The pancake density in the chain can not be directly fixed in experiment. Instead, the magnetic field strength, H_z, fixes the chemical potential μ_H, $\mu_H = \Phi_0 H_z/(4\pi)$, and the equilibrium density is determined by the global minimum of the thermodynamic potential $G(n) = E(n) - \mu_H n$. To find the density evolution with increasing the chemical potential, we plot in Fig. 5(left) the density dependencies of the reduced thermodynamic potential, $\delta\mathcal{E} - \mu n$ for different μ and representative parameters $N = 14$ and $\alpha = 0.6$. As the energy of isolated stacks is subtracted in $\delta\mathcal{E}$, the dimensionless chemical potential is shifted with respect to its bare value and it is related to the magnetic field strength as $\mu = N\Phi_0(H_z - H_{c1})/(4\epsilon_0)$, where H_{c1} is the lower critical field for $\mathbf{H}\|c$. We find that for selected parameters the transition takes place at $\mu = \mu_t = -6.668$. At $\mu < \mu_t$ the global minimum falls into the region of kinked lines and at $\mu > \mu_t$ it jumps into the region of crossing chain. Note that the density value, at which the energy curves cross (kinks in the lines in Fig. 5), is always larger than the lower density from which the jump to the high-density state takes place. At the transition, the density

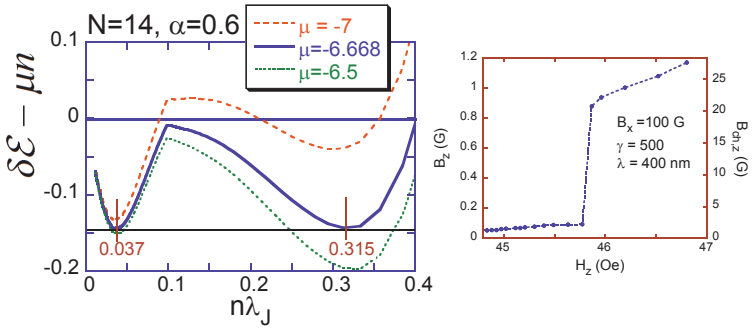

Fig. 5. *Left plot* shows the density dependence of the pancake part of the thermodynamic potential per unit area, $\delta\mathcal{E} - \mu n$ (in units of $\epsilon_0/(\pi\lambda_J N)$) at different values of chemical potential μ corresponding to different external fields for $N = 14$ and $\alpha = 0.6$. Kinks in the curves separate regions of tilted/kinked lines (low n) and crossing chains (high n). The equilibrium density is given by the global minimum of this energy. One can see that at $\mu \approx -6.668$ the system experiences a first-order phase transition with very large density jump. *Right plot* shows the corresponding dependencies of the average magnetic induction, B_z, (left axis) and the maximum induction in the middle of the chain, $B_{ch,z}$, (right axis) vs the magnetic field strength, H_z.

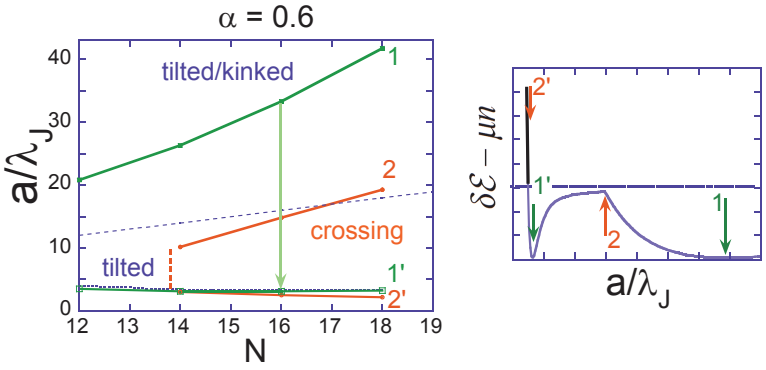

Fig. 6. *The left panel* shows the phase diagram in the N-a plane for $\alpha = 0.6$. *The right panel* illustrates definitions of the phase lines using the plot of the thermodynamic potential $\delta\mathcal{E} - \mu n$ vs a/λ_J at the transition point. The lines 1 and $1'$ correspond to the two limiting pancake separations at the transition point between which the jump occurs. The line 2 indicates crossing of the energy curves for the kinked and crossing chain. The line $2'$ shows position of the continuous transition into the tilted chain. Dotted line slightly above $1'$-line shows position of the maximum equilibrium separation a_m. We also show by the dashed line the crossover line $a/\lambda_J = N$ above which well-defined kinks appear.

jumps almost ten times, from $0.037/\lambda_J$ to $0.315/\lambda_J$. The right plot in Fig. 5 shows the corresponding dependencies of the average magnetic induction, $B_z = \Phi_0 n/c_y$, (left axis) and the maximum induction in the middle of the chain, $B_{ch,z} = \Phi_0 n/\lambda$, (right axis) vs the magnetic field strength, H_z. One can see that the jump in B_z occurs from ~ 0.1G to ~ 1G.

The numerically obtained phase diagram in the N-a plane for $\alpha = 0.6$ is shown in the left panel of Fig. 6. The plot of the thermodynamic potential at the transition point in the left panel illustrates definitions of different lines in the phase diagram. The lines 1 and $1'$ show the limiting pancake separations at the first-order transition between which the jump takes place. When the chemical potential is fixed by external conditions the area between these lines is bypassed in equilibrium. The line 2 inside this region marks the crossing of the energy curves for the two states. At large N the jump takes place from the kinked-lines state into the strongly corrugated configuration. This configuration transforms into the tilted chain with further decrease of a via continuous transition shown by the line $2'$. Below $N = 14$ only tilted chains realize, but the density jump still exists. The upper separation grows approximately proportional to N while the lower separation slowly decreases with N and lies slightly below the maximum equilibrium separation a_m shown by a dotted line. This means that the relative density jump increases with N. This type of phase diagram exists within a finite range of α, roughly $0.5 \lesssim \alpha \lesssim 0.7$. At larger α's only tilted chains exist.

6. CONCLUSIONS

In conclusion, we investigated the phase diagram of an isolated vortex chain in layered superconductors. In the region where Josephson and magnetic coupling are approximately equal, we found a very rich behavior. The crossing chains typically transform into the tilted chains with decreasing pancake separation via formation of intermediate strongly deformed configurations and continuous phase transition. When the relative strength of the Josephson coupling exceeds some typical value, the phase diagram becomes reentrant. At very small c-axis field, tilted chains are realized in which the vortex lines have kinked structure. With increasing the c-axis field these low-density tilted chains transform via a first-order phase transition into the strongly-deformed crossing chains. This transition is accompanied by a large jump of pancake-vortex density. With further field increase these crossing chains transform back into the tilted chains via a second-order transition.

7. ACKNOWLEDGEMENTS

I would like to thank M. Dodgson, A. Grigorenko, S. Bending, and V. Vlasko-Vlasov for useful discussions and the referee A for improving presentation. I also gratefully acknowledge use of "Jazz", a 350-node computing cluster operated by the Mathematics and Computer Science Division at Argonne National Laboratory as part of its Laboratory Computing Resource Center. This work was supported by the U. S. DOE, Office of Science, under contract # W-31-109-ENG-38.

REFERENCES

1. A. I. Buzdin and D. Feinberg, J. Phys. (Paris) **51**, 1971 (1990); S. N. Artemenko and A. N. Kruglov, Phys. Lett. A **143** 485 (1990); J. R. Clem, Phys. Rev. B **43**, 7837 (1991).
2. B. I. Ivlev, Yu. N. Ovchinnikov, and V. L. Pokrovsky, Mod. Phys. Lett.,**5**, 73 (1991).
3. L. N. Bulaevskii, M. Ledvij, and V. G. Kogan, Phys. Rev. B **46**, 366 (1992).
4. D. Feinberg and A. M. Ettouhami, Int. J. Mod. Phys. B **7**, 2085 (1993).
5. A. E. Koshelev, Phys. Rev. B **48**, 1180 (1993).
6. A. I. Buzdin and A. Yu. Simonov, JETP Lett. **51**, 191 (1990); A. M. Grishin, A. Y. Martynovich, and S. V. Yampolskii, Sov. Phys. JETP **70**, 1089 (1990); B. I. Ivlev and N. B. Kopnin, Phys. Rev. B **44**, 2747 (1991); W. A. M. Morgado, M. M. Doria, and G. Carneiro, Physica C, **349**, 196 (2001).
7. L. L. Daemen *et al.*, Phys. Rev. Lett. **70**, 2948 (1993); A. Sudbø, E. H. Brandt, and D. A. Huse Phys. Rev. Lett. **71**, 1451 (1993); E. Sardella, Physica C **257**, 231 (1997).
8. A. E. Koshelev, Phys. Rev. Lett. **83**, 187 (1999).
9. C. A. Bolle *et al.*, Phys. Rev. Lett. **66**, 112 (1991); I. V. Grigorieva *et al.*, Phys. Rev. B **51**, 3765 (1995).
10. A. Buzdin and I. Baladié, Phys. Rev. Lett. **88**, 147002 (2002).
11. T. Matsuda *et al.*, Science,**294**, 2136(2001).
12. A. Grigorenko *et al.*, Nature **414**, 728 (2001).
13. M. J. W. Dodgson, Phys. Rev. B **66**, 014509 (2002).
14. A. E. Koshelev, Physica C, **408-410**, 470 (2004).
15. M. Benkraouda and J. R. Clem, Phys. Rev. B **53**, 438 (1996).
16. A. M. Thompson and M. A. Moore, Phys. Rev. B **55**, 3856 (1997).